NANO LETTERS
Letter
Cite This: Nano Lett. 2018, 18, 7066−7074
pubs.acs.org/NanoLett

Poor Man's Atomic Layer Deposition of LiF for Additive-Free Growth of Lithium Columns

Wesley Chang,[†,‡] Jeung Hun Park,[†,‡] and Daniel A. Steingart*[,†,‡,§]

[†]Andlinger Center for Energy and the Environment, [‡]Department of Mechanical and Aerospace Engineering, and [§]Department of Chemical and Biological Engineering, Princeton University, Princeton, New Jersey 08544, United States

Supporting Information

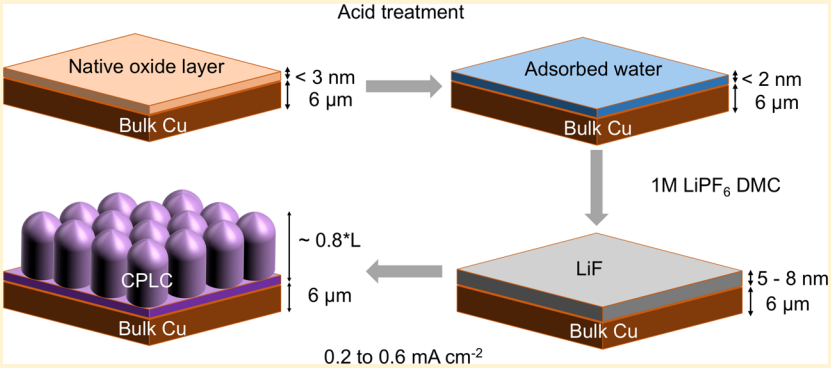

ABSTRACT: Lithium metal is an ideal material for high-energy, cost-effective rechargeable energy storage systems. The thermodynamically unfavorable solid−liquid interface between the lithium metal and organic electrolyte necessitates the formation of an interlayer (SEI) which is known to have significant impact on lithium morphologies. Less well understood is the impact of the current collector substrate on the morphology of electrodeposited lithium. Here we report on the morphology of electrodeposited lithium as a function of the chemical pretreatments of the working electrode. We find that a copper substrate pretreatment with acidic solutions (sulfuric, oxalic, or acetic acid) results in the deposition of close-packed lithium columns with a uniform diameter. A controlled study of the pre-electrodeposited copper surface indicates that the formation of a 5−8 nm thick LiF protective layer on copper substrate from a chemical reaction between adsorbed surface water layer in acidic solutions and $LiPF_6$ electrolyte is the key process in the electrochemical growth of lithium columns. We anticipate that this simple chemical approach can be generalized as a scalable, low-cost, additive-free substrate treatment method for depositing a LiF protective layer, broadly applicable in the development of uniform lithium films.

KEYWORDS: *Lithium metal anode, copper current collector, LiF layer, electrodeposition, surface treatment, close packed columnar growth*

Lithium metal is considered the ultimate negative electrode for high energy density rechargeable batteries due to its high theoretical specific capacity (3860 mAh g^{-1}) and strong chemical reducing ability (−3.04 V vs standard hydrogen electrode). The lithium-ion "rocking chair" design of secondary batteries, where lithium is de/inserted into host materials, has been critical for advancing the commercial state-of-the-art while providing critical insights into the consumption of electrolyte to stabilize interfaces within the battery.[1,2] However, the energy density of the graphite anode in commercial systems is approaching its theoretical limits, and ever-hungry applications from portable electronics to electric vehicles have compelled a recent resurgence in lithium metal battery research.[3−7] These efforts have focused on understanding the evolution of electrodeposited lithium metal over many plating and stripping cycles and then developing new nanoscale materials engineering techniques to inhibit or reduce unwanted growth (ramified, mossy, or dendritic) stemming from the inherent crystallography and reactivity of lithium.[8−16] Uniform lithium films can mitigate the anisotropic growth effects of varying current distribution along the surface, and therefore initial uniformity of the lithium anode material is important for prolonging the cycle life of rechargeable lithium metal batteries. It is possible to electrodeposit self-aligned lithium columns, a morphology which has been attributed to the LiF-rich interfacial layer.[14,17−23] This columnar growth has been observed with the use of several electrolyte additives[17,18] and with the use of aqueous electrolyte[14] for LiF nanoparticle surface coatings.[19] The apparent importance of a LiF-rich interfacial layer to uniform lithium deposition has also led to the artificial growth of a conformal LiF layer via atomic layer deposition (ALD).[16] The complexity of these nanoscale

Received: July 26, 2018
Revised: September 24, 2018
Published: October 8, 2018

DOI: 10.1021/acs.nanolett.8b03070
Nano Lett. 2018, 18, 7066−7074

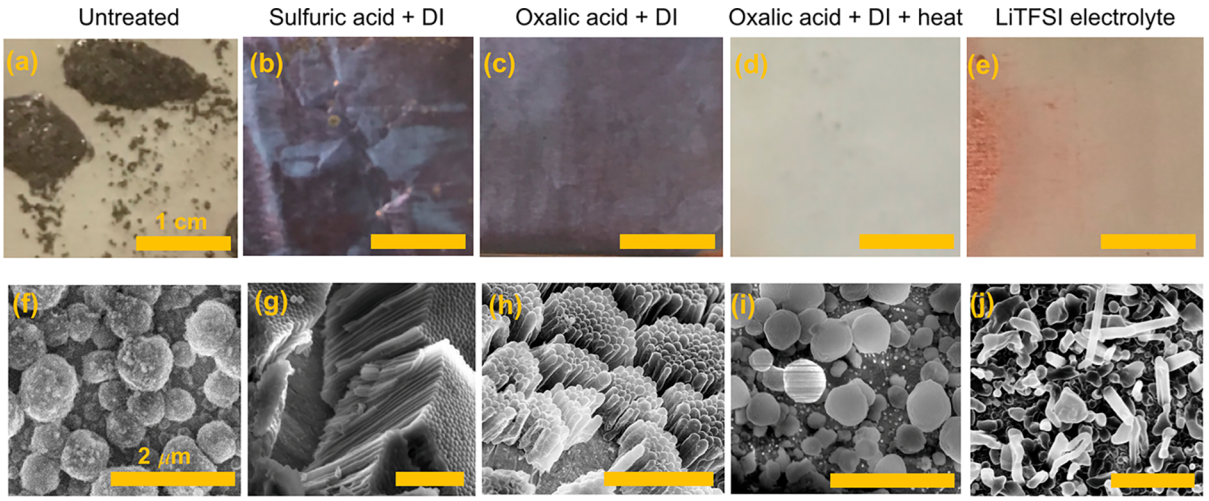

Figure 1. Optical images of lithium electrodeposited on Cu with various pretreatment conditions in 1 M $LiPF_6$ DMC (a) as-received, (b) sulfuric acid with deionized water rinse, (c) oxalic acid with deionized water rinse, (d) oxalic acid + deionized water + heat treatment at 200 °C for 2 h in vacuum oven, (e) oxalic acid + deionized water rinse in 1 M LiTFSI/LiBOB EC/DMC, and corresponding SEM images (f) spherical/mossy deposits of as-received Cu, (g) CPLC growth from sulfuric acid treated Cu, (h) CPLC growth from oxalic acid treated Cu, (i) spherical deposits of acid + 200 °C heat treated Cu, and (j) nodular structures of deposition in LiTFSI/LiBOB electrolyte.

materials engineering techniques suggests the desirability for a simpler and scalable process for uniform lithium deposition.

In this Letter, we report a simple electrodeposition process to control the morphology of lithium nanostructures that requires a slight modification of the electrolyte reduction on a metal substrate. We demonstrate an optimal method utilizing a simple acid treatment (for example, 95−98% sulfuric acid, or 3% acetic acid) with a deionized water rinse which foregoes the need to make changes to the bulk electrolyte or solid electrolyte interphase. The formation of a LiF-rich interface layer via in situ hydrolysis of adsorbed water and $LiPF_6$ electrolyte at the copper surface allows for uniform deposition of lithium. Xie et al.[16] first demonstrated the artificial formation of highly uniform LiF layers via ALD, which produced smooth lithium deposits. While our bulk current collector surface treatment similarly results in smooth lithium plating absent of ramified growth, the uniformity of the LiF interface layer may be compromised due to the lower precision of bulk surface pretreatment. By sacrificing the precision of ALD for the lower cost and simplicity of a bulk surface pretreatment, this approach is in effect a "poor man's ALD" of LiF. Our approach is compatible for a variety of conventional and engineered current collectors and may with optimization produce a reasonable route to a secondary lithium metal anode.

To explore the effect of copper substrate surfaces on lithium deposition, copper substrates first undergo a variety of surface treatment processes and are then immersed in the $LiPF_6$ electrolyte to observe the effect of each surface treatment process on the electrolyte/current collector surface. In order to remove surface contaminants and the native oxide layer from as-received copper (Goodfellow Oxygen Free High Conductivity, purity: 99.95+%, 6 μm thick), various pretreatments are utilized including acetone rinsing, Ar/O_2 plasma etching, and acid treatment. After treating the copper substrate, lithium is galvanostatically deposited in an argon filled glovebox via a flow cell setup adapted from Mashtalir et al.[23] A high current pulse at short duration (3.33 mA cm^{-2} for 2 s) nucleates a seed layer, and subsequent growth occurs at a lower current deposition rate (between 0.22 and 0.67 mA cm^{-2}) (Figure S1).

From Figure 1, visual differences from optical images (Figure 1a−e) can be correlated to morphological differences observed in the scanning electron microscopy (SEM) images (Figure 1f−j). Lithium deposited on untreated, as-received copper results in dark gray films with large black areas (Figure 1a). The gray areas correlate with spherical nanostructures (Figure 1f) with an average diameter of ∼420 ± 10% nm (as measured by SEM analysis using ImageJ software; other nanostructure measurements are shown in Figure S2), while the black areas contain mossy and ramified lithium growth. The black uneven areas, hypothesized to be due to nonuniform current distribution and/or heterogeneous surface reactions from surface impurities, are reduced/eliminated on copper that has been rinsed with deionized water (Figure S3). A deionized water rinse, an acetone rinse, and plasma cleaning all contribute to more uniform gray films but none are effective in removing the native oxide layer (Figure S4). For a stronger surface treatment, concentrated sulfuric acid (95−98% w/v) is used to etch away the native oxide layer, and results in columnar growth (heretofore known as close-packed lithium columnar morphology, or CPLC) (Figure 1b,g). Because of the corrosive nature of concentrated sulfuric acid, milder acids that are known to be effective for treating copper surfaces are also used.[24−26] Both oxalic acid (10% w/v) (Figure 1c,h) and acetic acid (3% w/v) result in the same CPLC morphology. CPLC growth is observed for low current deposition rates (between 0.22 and 0.67 mA cm^{-2}) with greater than 0.7 mA cm^{-2} resulting in black, ramified growth. The columnar nanostructures have hemispherical tips with ∼250 ± 10% nm measured diameter (Figure S2). Note that subsequent analyses of acid treated copper in this Letter use results from oxalic acid treatments.

Imaging at the initiation of deposition (t = 5 s) shows spherical lithium nucleates at the surface (Figures S5a). Later images depict longer, self-aligned, and compact rods of lithium (Figure S5b). The thickness of the columnar film grows linearly with charge passed as expected with Faradaically controlled growth. Estimation through SEM analysis indicates the expected thickness is achieved within an error of ±10%. The error can be attributed to an unknown amount of non-

DOI: 10.1021/acs.nanolett.8b03070
Nano Lett. 2018, 18, 7066−7074

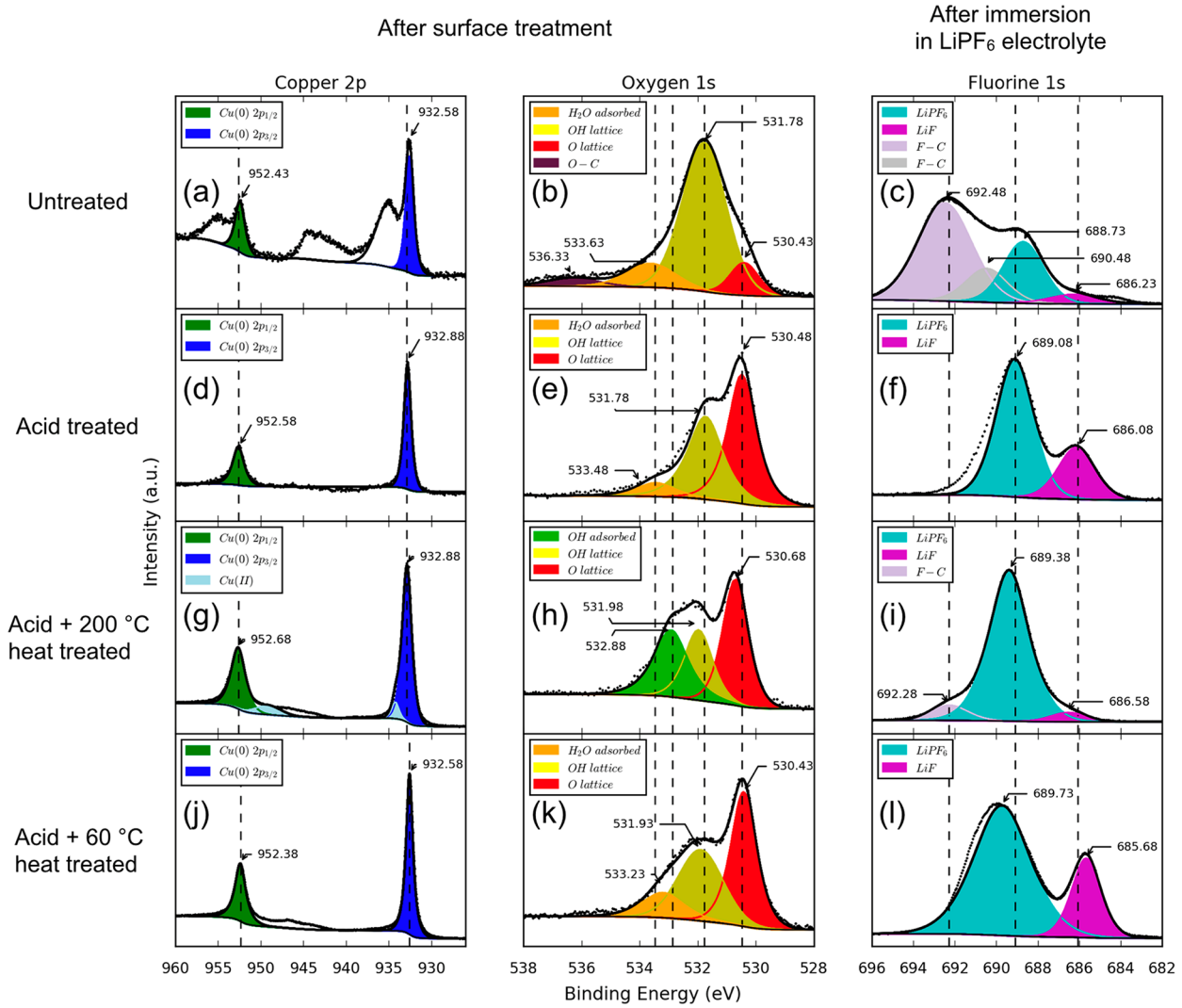

Figure 2. XPS Cu 2p scan (a) and O 1s scan (b) for as-received Cu, and F 1s scan (c) for as-received Cu after immersion in 1 M $LiPF_6$ DMC electrolyte. Similar scans for oxalic acid + deionized water treated Cu are shown in (d–f). Similar scans for oxalic acid + deionized water + high heat treated (200 °C, 2 h, in vacuum oven) Cu are shown in (g–i). Similar scans for oxalic acid + deionized water + mild heat treated (60 °C, 2 h, in vacuum oven) Cu are shown in (j–l).

Faradaic reaction products between the electrolyte and the lithium electrode. If this layer is washed off, the deposited film thickness will be overestimated by Faraday's law. Lithium films of greater than 25 μm thick have been deposited without complications, demonstrating the robustness of the surface pretreatment for long duration platings.

Because of the partial drying of the acid-treated copper before transferring into the glovebox for lithium plating, it is hypothesized that the acid + deionized water treatment process adsorbs surface water in addition to etching the native oxide. The surface water layer may react with $LiPF_6$ to form LiF via the decomposition reaction[27−29]

$$LiPF_6 + H_2O \rightarrow LiF + 2HF + POF_3 \quad (1)$$

This is similar to the previous literature by Qian et al. describing the use of trace amounts of water (25 to 50 ppm) to decompose $LiPF_6$ and form a LiF layer for uniform lithium growth.[14] It is well-known that $LiPF_6$ hydrolyzes easily, and that a major decomposition product in the presence of water is LiF.[20,27−29] Therefore, we would expect that the surface treatment procedure readily forms LiF at the surface by adsorbing surface water, avoiding the nontrivial addition of parts-per-million quantities of water in the electrolyte. To validate the adsorbed water hypothesis, the presence and absence of each reactant in eq 1 can be controlled to observe the effect on the formation of a LiF layer. To remove surface adsorbed water, acid-treated copper is then subjected to treatment at high temperatures in a vacuum oven (200 °C, 2 h), resulting in gray lithium films with spherical morphology, of diameter ~420 ± 10% nm (Figure 1d,i). To confirm that contamination from heat treatment in the vacuum oven is negligible, acid-treated copper is treated at mild temperatures (60 °C), resulting in the CPLC growth (Figure S3). To remove the other reactant, $LiPF_6$, an electrolyte less prone to hydrolysis is used for lithium plating: lithium bis(trifluoromethanesulfonyl)imide with lithium bis(oxalato)borate in ethylene carbonate dimethyl carbonate (1 M LiTFSI/LiBOB EC/DMC).[30] Deposition in this electrolyte resulted in a dark gray film with nodular structures (Figure 1e,j). Even with a combination of treatments used (i.e., acid followed by plasma etch, plasma etch followed by acid treatment), it is observed that any surface treatment with

DOI: 10.1021/acs.nanolett.8b03070
Nano Lett. 2018, 18, 7066−7074

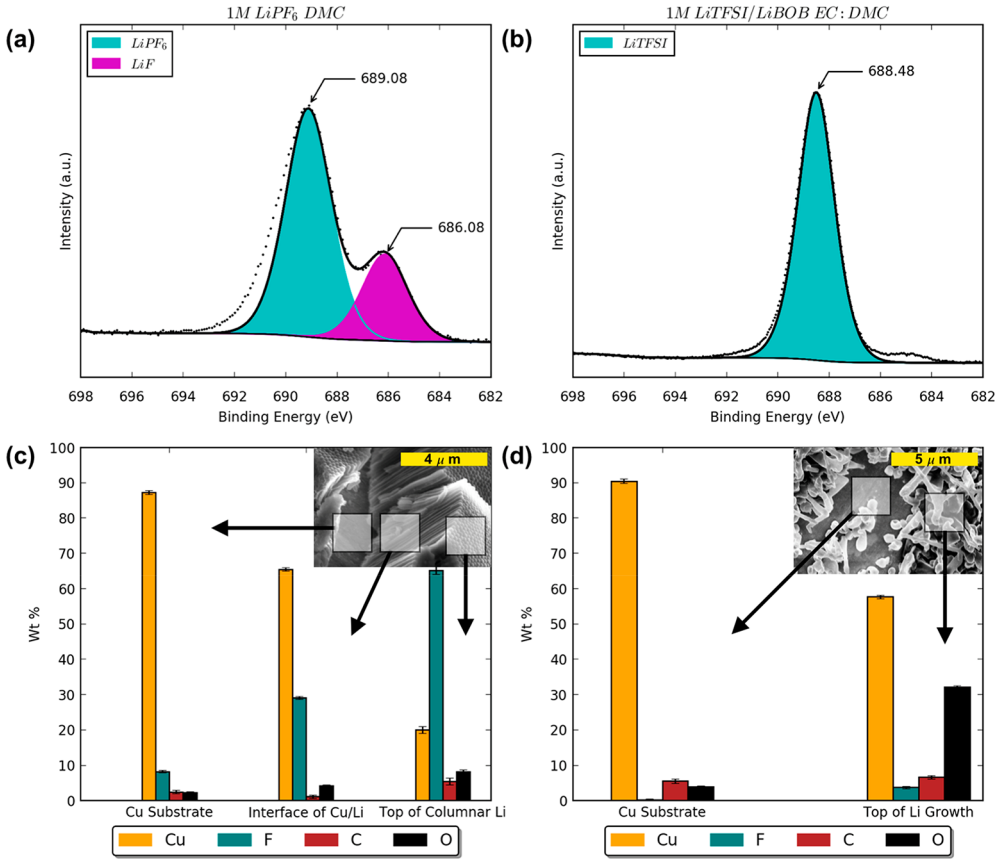

Figure 3. XPS F 1s spectrum of oxalic acid treated Cu immersed in (a) 1 M $LiPF_6$ DMC and (b) 1 M LiTFSI/LiBOB EC/DMC, and corresponding EDX elemental analysis of plated lithium films for (c) 1 M $LiPF_6$ DMC and (d) 1 M LiTFSI/LiBOB EC/DMC at various locations on the film/substrate.

acid + deionized water rinse as the last step results in the CPLC growth. Mild temperature treatment (60 °C) results in CPLC growth while high-temperature treatment (200 °C) results in spherical lithium. This observation suggests that the transition in morphology from CPLC to spherical deposits occurs at high temperatures and that contamination from the vacuum oven has a negligible effect on the plating morphology. Thus, the desorption of surface adsorbed water at high temperatures removes one of the reactants necessary for LiF formation and prevents the CPLC growth.

X-ray photoelectron spectroscopy (XPS) was used to detect a surface adsorbed water layer after copper surface treatment (Figure 2a,b,d,e,g,h,j,k), and a surface LiF layer after immersion of the treated copper in the $LiPF_6$ electrolyte (Figure 2c,f,i,l). First, XPS spectra of the as-received copper indicates broad and shakeup peaks in the Cu 2p scan corresponding to the native oxide layer (Figure 2a).[31] XPS depth profiling of the Cu 2p scan estimates this oxide layer to be less than 2 nm in thickness. The effectiveness of the acid treatment in removing the native oxide layer is shown by the well-defined peaks at 932.88 eV (Cu $2p_{3/2}$) and 952.58 eV (Cu $2p_{1/2}$), corresponding to metallic Cu (Figure 2d).[32] The other scans for untreated copper are shown but do not provide clear additional information because of the large amount of impurities in as-received copper (Figure 2b,c). More importantly, a slight difference between the O 1s scans of acid treated and acid + heat treated copper can be noted (Figure 2e,h). Peak deconvolution of the acid treated copper indicates a broadening at the higher binding energy side and the assignment of the additional peak at 533.48 eV to adsorbed surface water (Figure 2e).[33,34] It appears that the acid + heat-treated copper substrates retain the two distinct peaks assigned to metallic Cu but with wider fwhm values (1.06 eV for acid treated Cu $2p_{3/2}$ to 1.37 eV for acid + heat treated Cu $2p_{3/2}$; 1.72 eV for acid treated Cu $2p_{1/2}$ to 2.04 eV for acid + heat treated Cu $2p_{1/2}$) (Figure 2g). The wider fwhm values may be attributed to additional smaller copper oxide peaks upon peak deconvolution, suggesting reoxidation of the surface. This is confirmed by micro-Raman spectra, showing a blue-shifted peak with higher intensity (indicative of a more oxidized surface state) for acid + heat-treated copper relative to deionized water rinsed copper, and a red-shifted peak with broadening for acid-treated copper relative to deionized water rinsed copper (Figure S6).[35] Deconvolution of the O 1s scan for the acid + heat-treated copper indicates a peak at 532.88 eV, about 0.6 eV lower than the 533.48 eV peak in Figure 2e that is assigned to adsorbed water. The wider fwhm values in the Cu 2p scan and the different peak assignment in the O 1s scan indicates that while heat treatment retains bulk metallic Cu and evaporates surface water, it has also oxidized the surface. Deionized water rinsed and plasma-etched copper substrates both exhibit copper oxide peaks in the respective Cu 2p XPS scans (Figure S4), corresponding to gray films with spherical lithium morphology. The deionized water rinsed and plasma cleaned copper substrates seem to result in more uniform gray films than the as-received copper, perhaps due to the effective removal of surface contaminants.

DOI: 10.1021/acs.nanolett.8b03070
Nano Lett. 2018, 18, 7066−7074

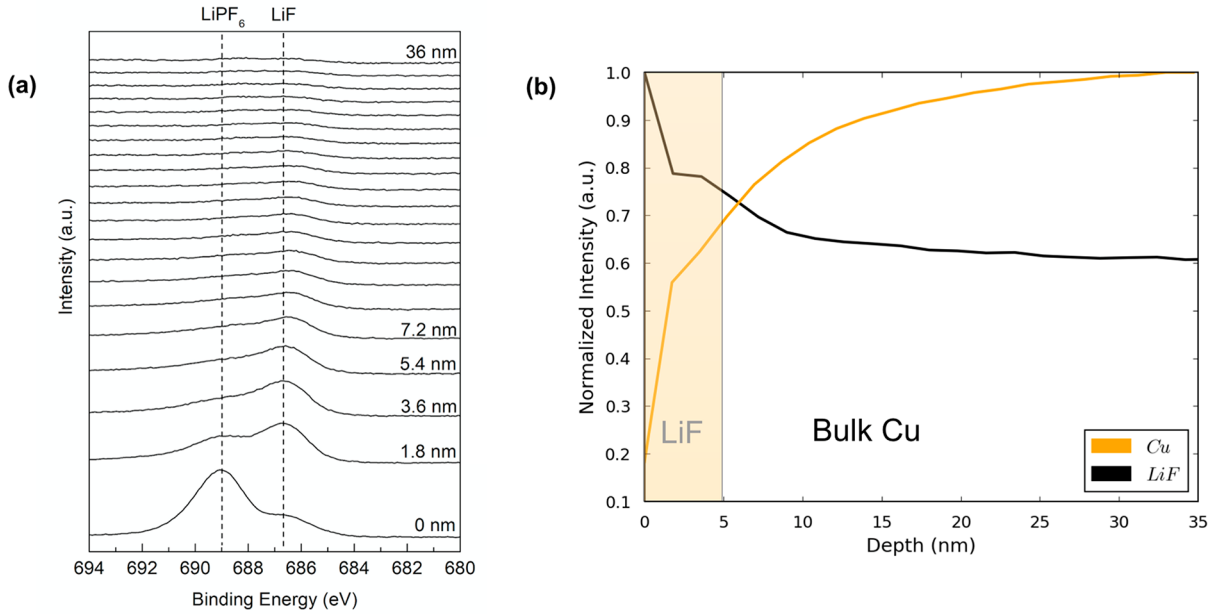

Figure 4. (a) A 2D cascade plot of depth-profiled XPS F 1s spectrum for oxalic acid treated copper immersed in 1 M $LiPF_6$ DMC, (b) normalized intensity as a function of etch distance for estimating LiF surface layer thickness.

As explained, the first two columns of Figure 2 correlate with the Cu 2p and O 1s scans of the treated copper substrate. The treated substrate is then immersed in the $LiPF_6$ electrolyte and transferred under inert atmosphere to the XPS loadlock chamber to characterize the electrolyte/substrate interface. The F 1s scan for acid treated copper indicates a peak at 686.08 eV corresponding to LiF (Figure 2f).[36−42] This peak is observed for samples treated with various acids as well as mild heat treated (60 °C) copper (Figure 2l) and never is observed for the acid + 200 °C heat treated samples (Figure 2i). There are no noticeable differences in the XPS scans of the acid treated copper and acid + mild heat treated copper, which both result in CPLC growth morphology. The other peak at 689.08 eV appears for all samples and is assigned to the $LiPF_6$ electrolyte.[43,44] Similar peaks appear in the deconvolution of the as-received copper, due to the effects of sitting in ambient atmosphere (i.e., collecting of water molecules and reaction of surface contaminants with electrolyte). While Qian et al. observed the $LiPF_6$ decomposition process to take hours, prior studies also indicated that decomposition may be sped up by the presence of H^+; this may explain why we detect LiF in our acid treated copper substrates after immersing in $LiPF_6$ for 15 s.[14,28]

The C 1s and O 1s scans of the Cu substrates after immersion in $LiPF_6$ electrolyte indicate the presence of alkyl carbonates and hydrocarbons (Figure S7). The hydrocarbon peak at ∼284.6 eV is always observed in C 1s scans due to carbon contamination; the alkyl carbonates (ROLi, $-CO_3$, $-CO_2$) may be further byproducts from the decomposition of DMC solvent in the presence of trace oxides or hydroxides on the copper surface.[17,23,41] The combined results from the XPS scans after surface treatment and immersion in $LiPF_6$ indicate that the major components of the interfacial layer on copper in 1 M $LiPF_6$ DMC, but before Li plating, are LiF, alkyl carbonates, and hydrocarbon.

The heat treatment process removes one of the reactants, that is, the surface adsorbed H_2O layer. Figure 2 showed the presence of surface-adsorbed water after surface treatment of copper, and the presence of a LiF layer after subsequent immersion in the $LiPF_6$ electrolyte. Similar indication of the presence and absence of the LiF layer for $LiPF_6$ and non-$LiPF_6$ electrolyte, respectively, is shown in Figure 3. The resulting lithium deposition produces dark gray films with nodular and ramified growth throughout. This may be attributed to the lack of LiF formation due to LiTFSI being less prone to hydrolysis than $LiPF_6$. Energy-dispersive X-ray spectroscopy (EDX) elemental analysis indicates insignificant amounts of fluorine on the nodular lithium films (<5 wt %) in contrast with significant amounts of fluorine (>70 wt %) found on top of the CPLC films (Figure 3c,d). Analysis of various areas on a cross-sectional SEM image of the CPLC indicates increased fluorine content on top of the films versus the copper substrate base or copper/lithium interface (Figure 3c). XPS confirms the presence of a LiF peak at 686.08 eV for acid treated copper in 1 M $LiPF_6$ DMC and the absence of the LiF peak for acid treated copper in 1 M LiTFSI/LiBOB EC:DMC (Figure 3a,b).[36−42] The other peak at 689.08 eV, which is present in both electrolytes, is assigned to a thin surface electrolyte layer.[43,44] This electrolyte layer is present because the samples were not rinsed or dried after immersion in electrolyte so that the surface electrolyte may aid as a protective layer for the reactive LiF.

After validating the disappearance of the LiF layer in copper substrates that were subject to high-temperature treatment or immersed in LiTFSI electrolyte, the thickness of the LiF layer was quantified for the acid-treated samples, as this thickness dictates the surface interfacial resistance and lithium diffusivity. With XPS depth profiling, the LiF peak was observed to disappear within the first 5−8 nm (Figure 4b). The initial pre-etch F 1s scan (Figure 4a) indicates a large presence of $LiPF_6$ at 689.0 eV, which is attributed to the fact that the sample was not rinsed after electrolyte immersion. Upon etching, this $LiPF_6$ peak disappears with the LiF peak at ∼686.5 eV fading away at a slower rate.

From the experimental results provided, a proposed mechanism for the effect of pretreatment on CPLC growth

DOI: 10.1021/acs.nanolett.8b03070
Nano Lett. 2018, 18, 7066−7074

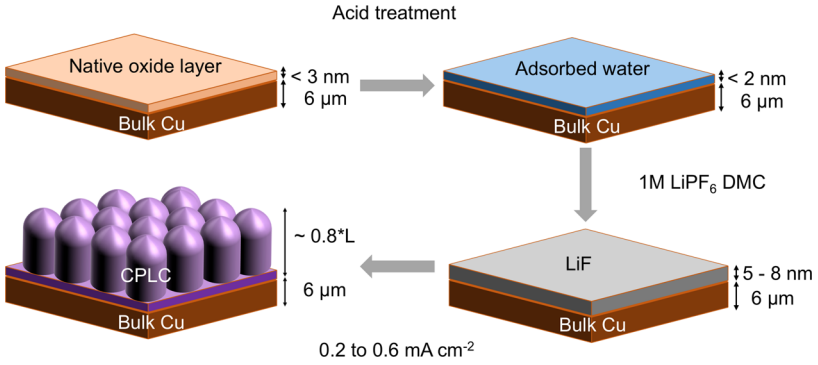

Figure 5. Schematic of the proposed mechanism for the acid treatment of Cu current collector that deposits a surface LiF layer and results in close-packed columnar lithium growth. The thickness of the deposited lithium is observed to be approximately 0.8*L, where L is the theoretical thickness derived from charge passed, assuming close-packed lithium. For example, Figure 6a depicts an SEM image of Li columns deposited at a plating current density of 0.33 mA cm^{-2} for a total plating duration of 3 h. This results in the theoretical thickness of (1 mAh cm^{-2}/26801 mAh mol^{-1}) × (6.941 g mol^{-1}/0.534 g cm^{-3}) = 4.85 μm, and an observed thickness of ~4 μm, which is about 80% of the theoretical.

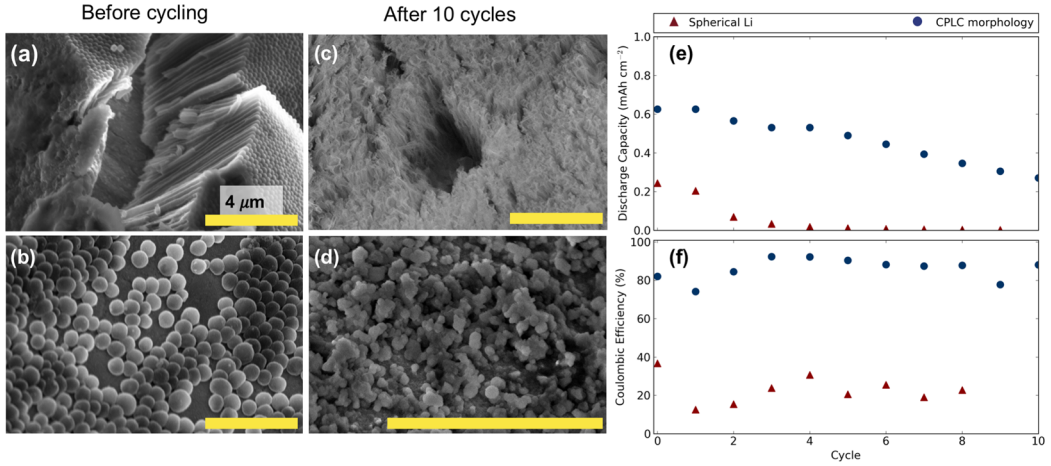

Figure 6. SEM images of pristine (a) CPLC growth (1 mAh cm^{-2}) on acid-treated copper, and (b) spherical deposits (1 mAh cm^{-2}) on acid + 200 °C heat-treated copper; SEM images of (c) CPLC growth and (d) spherical deposits after 10 cycles at 0.1 mA cm^{-2}; (e) areal discharge capacity of CPLC and spherical growth and (f) corresponding Coulombic efficiency (%) defined by discharge capacity/charge capacity. Note: all scale bars correspond to 4 μm.

is depicted in Figure 5. Acid treatment with a deionized water rinse removes the native copper oxide layer and surface impurities, while adsorbing a surface water layer, as evidenced by XPS of acid treated samples. The surface water layer reacts with the aprotic electrolyte (1 M $LiPF_6$ DMC) to form a surface LiF layer, as evidenced by XPS of acid treated samples immersed in the electrolyte. The presence of the LiF peak in the XPS F 1s scan is unique to the acid-treated copper in $LiPF_6$ electrolyte, which is also correlated one to one with CPLC growth.

The effectiveness of the acid pretreatment in removing the surface copper oxide layer and adsorbing a surface water layer has been shown. There are two reactants in the decomposition of $LiPF_6$ in water, $LiPF_6$ and H_2O. Heat treatment to high temperature was used to remove H_2O, resulting in absence of a LiF layer and spherical rather than columnar lithium. Electrolyte substitution was used to remove the other reactant, $LiPF_6$, also resulting in absence of fluorine and a different lithium morphology.

In order to develop a stronger correlation between the various growth morphologies of lithium and the electrochemical cycling performance for the application of rechargeable battery anodes, the capacity retention and Coulombic efficiency (CE) were examined (Figure 6e,f). Mossy/spherical deposits from untreated copper, CPLC morphology from acid treated copper, and spherical deposits from acid + heat-treated copper were discharged at 0.05 mA cm^{-2} into a fully delithiated $LiFePO_4$ electrode in order to determine the initial discharge capacity. They were then repeatedly charged and discharged for 10 cycles at a constant current of 0.1 mA cm^{-2} in the voltage range of 2.8−4 V versus Li^+/Li. The mossy/spherical growth of untreated copper was unable to be discharged at all. The spherical deposits of acid + heat treated copper only retained ~20% of the lithium loading upon discharge (Figure 6b,d). However, the acid treated copper with CPLC morphology discharged over 60% of the theoretical thickness (Figure 6a,c). Surface treatment with acid, which results in the CPLC morphology and LiF-rich interface, also exhibits 80% CE which is a significant improvement over LiF-absent copper surfaces (Figure 6f). The improvement in plating/stripping efficiency may be due to the lower surface area achieved by compact columnar growth and effects of the LiF layer, relative to spherical Li deposits (Figure 6a,b). However, the SEM image of the CPLC after 10 cycles (Figure 6c) indicates that the columns are less compact and appear to be covered with substantial interphase layers; optimization of

DOI: 10.1021/acs.nanolett.8b03070
Nano Lett. 2018, 18, 7066−7074

the CPLC porosity and density for additional enhancement of the CE is left for a future study.

We have utilized a common industrial cleaning process for etching native oxide layers from copper to demonstrate an additive-free method for LiF interface formation. The acid treatment of copper is akin to a "poor man's atomic layer deposition" of LiF via electrolyte reduction by surface adsorbed water. This wafer-scale treatment process avoids the cost of electrolyte additives or the nontrivial addition of bulk water in the electrolyte. The subsequent uniform growth of thin lithium films may be used as rechargeable lithium metal anodes with further optimization of electrolyte and lithium deposition morphology for improved cycling efficiency.

Methods. *Treatment of Copper.* OFHC (purity >99.95%) copper was purchased from Goodfellow (hard temper, 6 μm thick). Copper foil was cut into strips 3 cm wide. The foil was immersed in an acid bath, using concentrated sulfuric acid (95−98%, Sigma-Aldrich), oxalic acid (10% w/v, Sigma-Aldrich), or acetic acid (3% w/v, Sigma-Aldrich) for 30 s. The foil was then rinsed in deionized water to wash away the acid, and dried with a Kimwipe to remove bulk liquid on the surface. The foil was transferred inside sealed containers into an Ar-filled glovebox with O_2 levels <0.7 ppm and H_2O levels <0.2 ppm.

Electrolyte Synthesis. Lithium bis(trifluoromethane)-sulfonimide (LiTFSI) and lithium bis(oxalato)borate (LiBOB) were purchased from Sigma-Aldrich. LiTFSI and LiBOB were heated in the large vacuum antechamber at 140 °C overnight for complete drying. LiBOB (0.5 M) was dissolved in ethylene carbonate (EC) at elevated temperature (~60−100 °C) while stirring. LiTFSI (0.5 M) was then added along with 5 mL of dimethyl carbonate (DMC) for a 10 mL solution. The solution was stirred at room temperature overnight, resulting in 1 M LiTFSI/LiBOB EC/DMC (1:1 wt %) electrolyte to be used for plating studies.

Electrodeposition of Lithium. Lithium was electrodeposited using a modified version of an aqueous electrolyte deposition system developed by Alpha-En Corporation. A flowing aqueous electrolyte containing lithium carbonate, sulfuric acid, and deionized water was started with a pump at 1800 rpm. The Ag/AgCl reference electrode was connected into a tank containing the aqueous electrolyte, which is distributed into the glovebox through tubing. Inside the glovebox, the treated copper foil was placed onto a sample holder that was immersed in 1 M $LiPF_6$ DMC. The nonaqueous and aqueous electrolytes were separated by the lithium-ion conducting glass-ceramic membrane (LICGC, Ohara Corp). A schematic of the setup can be found in Mashtalir et al.[23] Electrodeposition experiments were conducted galvanostatically with a potentiostat (Reference 3000, Gamry Instruments) with current densities ranging from −0.22 to −0.67 mA cm^{-2} to obtain CPLC morphology. An initial seed layer was deposited with a higher current density (−3.33 mA cm^{-2}). The voltage increased to −10 V during the high current seed step then decreased to −3 to −5 V versus Ag/AgCl during the low current growth phase. Typical plating duration was 1 h with duration up to 11 h being successful.

Characterization. Samples were rinsed in DMC and dried in the large vacuum antechamber of the glovebox at 40 °C for 2 h before characterization. SEM samples were transferred via double containers filled with argon from the glovebox and were exposed to air for less than 5 s with evacuation of the load lock being almost instantaneous (a few seconds). SEM images were collected on a Verios 460 XHR SEM with an accelerating voltage of 5 keV and a working distance between 3 and 4 mm. Cross-sectional images were taken by cutting a sample foil with shears and using a 45° sample holder. An attached X-ray detector (Oxford Instruments) was used for EDX analysis. AZtec software was used for EDX elemental analysis. XPS analysis was performed using a Thermo Scientific K-Alpha instrument with an Al Kα source and 400 μm spot size (0.05 eV step size for core-level scans, 1 eV for survey scans). The operating pressure was <8.0×10^{-8} Torr, and the sample was transferred via a vacuum sample holder and never exposed to atmosphere. The Au $4f_{7/2}$ peak at 84.00 eV from a thermally evaporated 300 nm thick Au/Si(111) substrate was used as a reference for charge shift correction of the binding energy. Avantage software was used for the least-squares fitting of XPS spectra with Lorentzian−Gaussian line shape (30% L/G mix for F 1s scans, 80% for O 1s, and 80% for Cu 2p) and a Shirley background subtraction. Depth profiling was carried out with an Ar ion gun (2 keV, monatomic, 400 μm spot size) for a series of 20 etches of 30 s each (10 min total). The following equation was used to back calculate the ion current from SiO_2 reference values and to then calculate the LiF etch rate in nm/min[45−47]

$$z/t\ (\mathrm{nm/min}) = \frac{M}{r^{*}\mathrm{NA}^{*}e}{}^{*}S^{*}jp$$

where M = molar mass of etched material, r = density of etched material, NA = Avogadro's number (6.022×10^{23} mol^{-1}), e = electron charge (1.6×10^{-19} A−s), S = sputter yield (atom/ion) from a table of reference values, and jp = ion beam current density.

Particle Size Measurements. Lithium nuclei diameters were approximated by ImageJ software, using gray value mappings for a given line scan to count particles and divide by the total distance measured. For 45° tilted samples, the distance was converted geometrically to obtain the actual distance.

■ ASSOCIATED CONTENT

Supporting Information

The Supporting Information is available free of charge on the ACS Publications website at DOI: 10.1021/acs.nanolett.8b03070.

Current/voltage information for galvanostatic electrodeposition experiments, lithium nanostructure diameter measurements using ImageJ software, additional optical and SEM images of plated lithium, additional XPS spectra of various copper substrates, and micro-Raman spectroscopy measurements of various copper substrates.(PDF)

■ AUTHOR INFORMATION

Corresponding Author

*E-mail: steingart@princeton.edu.

ORCID

Wesley Chang: 0000-0002-9389-1265
Jeung Hun Park: 0000-0002-8797-1293
Daniel A. Steingart: 0000-0002-8184-9641

Notes

The authors declare no competing financial interest.

DOI: 10.1021/acs.nanolett.8b03070
Nano Lett. 2018, 18, 7066−7074

■ ACKNOWLEDGMENTS

This work was supported by Alpha-En Corporation and Mercedes-Benz Research & Development North America, Inc. The authors thank Mr. Lawrence Swonger and Ms. Emilie Bodoin for technical advice on cell design and plating protocols. We thank Professor Bruce Koel for enlightening discussions on XPS peak fitting and analysis.

■ REFERENCES

(1) Dunn, B.; Kamath, H.; Tarascon, J. Electrical energy storage for the grid: a battery of choices. *Science* **2011**, *334*, 928−936.
(2) Goodenough, J. B.; Park, K. S. The Li-ion rechargeable battery: a perspective. *J. Am. Chem. Soc.* **2013**, *135*, 1167−1176.
(3) Xu, W.; Wang, J.; Ding, F.; Chen, X.; Nasybulin, E.; Zhang, Y.; Zhang, J.-G. Lithium metal anodes for rechargeable batteries. *Energy Environ. Sci.* **2014**, *7*, 513−537.
(4) Aurbach, D.; Zinigrad, E.; Cohen, Y.; Teller, H. A short review of failure mechanisms of lithium metal and lithiated graphite anodes in liquid electrolyte solutions. *Solid State Ionics* **2002**, *148*, 405−416.
(5) Aurbach, D.; Zinigrad, E.; Teller, H.; Dan, P. Factors which limit the cycle life of rechargeable lithium (metal) batteries. *J. Electrochem. Soc.* **2000**, *147*, 1274.
(6) Lin, D.; Liu, Y.; Cui, Y. Reviving the lithium metal anode for high-energy batteries. *Nat. Nanotechnol.* **2017**, *12*, 194−206.
(7) Cheng, X. B.; Zhang, R.; Zhao, C. Z.; Zhang, Q. Toward safe lithium metal anode in rechargeable batteries: a review. *Chem. Rev.* **2017**, *117*, 10403−10473.
(8) Ding, F.; Xu, W.; Graff, G. L.; Zhang, J.; Sushko, M. L.; Chen, X.; Shao, Y.; Engelhard, M. H.; Nie, Z.; Xiao, J.; Liu, X.; Sushko, P. V.; Liu, J.; Zhang, J. G. Dendrite-free lithium deposition via self-healing electrostatic shield mechanism. *J. Am. Chem. Soc.* **2013**, *135*, 4450−4456.
(9) Stark, J. K.; Ding, Y.; Kohl, P. A. Dendrite-free electrodeposition and reoxidation of lithium-sodium alloy for metal-anode battery. *J. Electrochem. Soc.* **2011**, *158*, A1100.
(10) Stark, J. K.; Ding, Y.; Kohl, P. A. Nucleation of electrodeposited lithium metal: dendritic growth and the effect of co-deposited sodium. *J. Electrochem. Soc.* **2013**, *160*, D337−D342.
(11) Zheng, G.; Lee, S. W.; Liang, Z.; Lee, H. W.; Yan, K.; Yao, H.; Wang, H.; Li, W.; Chu, S.; Cui, Y. Interconnected hollow carbon nanospheres for stable lithium metal anodes. *Nat. Nanotechnol.* **2014**, *9*, 618−623.
(12) Qian, J.; Adams, B. D.; Zheng, J.; Xu, W.; Henderson, W. A.; Wang, J.; Bowden, M. E.; Xu, S.; Hu, J.; Zhang, J.-G. Anode-free rechargeable lithium metal batteries. *Adv. Funct. Mater.* **2016**, *26*, 7094−7102.
(13) Qian, J.; Henderson, W. A.; Xu, W.; Bhattacharya, P.; Engelhard, M.; Borodin, O.; Zhang, J. G. High rate and stable cycling of lithium metal anode. *Nat. Commun.* **2015**, *6*, 6362.
(14) Qian, J.; Xu, W.; Bhattacharya, P.; Engelhard, M.; Henderson, W. A.; Zhang, Y.; Zhang, J. G. Dendrite-free Li deposition using trace-amounts of water as an electrolyte additive. *Nano Energy* **2015**, *15*, 135−144.
(15) Suo, L.; Hu, Y. S.; Li, H.; Armand, M.; Chen, L. A new class of solvent-in-salt electrolyte for high-energy rechargeable metallic lithium batteries. *Nat. Commun.* **2013**, *4*, 1481.
(16) Xie, J.; Liao, L.; Gong, Y.; Li, Y.; Shi, F.; Pei, A.; Sun, J.; Zhang, R.; Kong, B.; Subbaraman, R.; Christensen, J.; Cui, Y. Stitching h-BN by atomic layer deposition of LiF as a stable interface for lithium metal anode. *Sci. Adv.* **2017**, *3*, eaao3170.
(17) Zhang, Y.; Qian, J.; Xu, W.; Russell, S. M.; Chen, X.; Nasybulin, E.; Bhattacharya, P.; Engelhard, M. H.; Mei, D.; Cao, R.; Ding, F.; Cresce, A. V.; Xu, K.; Zhang, J. G. Dendrite-free lithium deposition with self-aligned nanorod structure. *Nano Lett.* **2014**, *14*, 6889−6896.
(18) Ren, X.; Zhang, Y.; Engelhard, M. H.; Li, Q.; Zhang, J. G.; Xu, W. Guided lithium metal deposition and improved lithium coulombic efficiency through synergistic effects of $LiAsF_6$ and cyclic carbonate additives. *ACS Energy Letters* **2018**, *3* (1), 14−19.
(19) Zhang, X. Q.; Chen, X.; Xu, R.; Cheng, X. B.; Peng, H. J.; Zhang, R.; Huang, J. Q.; Zhang, Q. Columnar lithium metal anodes. *Angew. Chem., Int. Ed.* **2017**, *56*, 14207−14211.
(20) Mehdi, B. L.; Stevens, A.; Qian, J.; Park, C.; Xu, W.; Henderson, W. A.; Browning, N. D.; et al. The impact of Li grain size on coulombic efficiency in Li batteries. *Sci. Rep.* **2016**, *6*, 1−8.
(21) Pei, A.; Zheng, G.; Shi, F.; Li, Y.; Cui, Y. Nanoscale nucleation and growth of electrodeposited lithium metal. *Nano Lett.* **2017**, *17*, 1132−1139.
(22) Lu, Y.; Tu, Z.; Archer, L. A. Stable lithium electrodeposition in liquid and nanoporous solid electrolytes. *Nat. Mater.* **2014**, *13*, 961−969.
(23) Mashtalir, O.; Nguyen, M.; Bodoin, E.; Swonger, L.; O'Brien, S. P. High-purity lithium metal films from aqueous mineral solutions. *ACS Omega* **2018**, *3*, 181−187.
(24) Aksu, S.; Doyle, F. M. Electrochemistry of copper in aqueous oxalic acid solutions. *J. Electrochem. Soc.* **2001**, *148*, B51−B57.
(25) Gabrielli, C.; Mace, C.; Matha, J.; Mège, S.; Ostermann, E.; Perrot, H. Investigation of dissolution and electrodeposition of copper in concentrated and diluted oxalic acid media in post-CMP cleaning. *Solid State Phenom.* **2005**, *103-104*, 287−290.
(26) Chavez, K. L.; Hess, D. W. A novel method of etching copper oxide using acetic acid. *J. Electrochem. Soc.* **2001**, *148*, G640.
(27) Guéguen, A.; Streich, D.; He, M.; Mendez, M.; Chesneau, F. F.; Novák, P.; Berg, E. J. Decomposition of $LiPF_6$ in high energy lithium-ion batteries studied with online electrochemical mass spectrometry. *J. Electrochem. Soc.* **2016**, *163*, A1095−A1100.
(28) Plakhotnyk, A. V.; Ernst, L.; Schmutzler, R. Hydrolysis in the system $LiPF_6$- propylene carbonate - dimethyl carbonate - H_2O. *J. Fluorine Chem.* **2005**, *126*, 27−31.
(29) Terborg, L.; Nowak, S.; Passerini, S.; Winter, M.; Karst, U.; Haddad, P. R.; Nesterenko, P. N. Ion chromatographic determination of hydrolysis products of hexafluorophosphate salts in aqueous solution. *Anal. Chim. Acta* **2012**, *714*, 121−126.
(30) Younesi, R.; Veith, G. M.; Johansson, P.; Edström, K.; Vegge, T. Lithium salts for advanced lithium batteries: Li-metal, Li-O_2, and Li-S. *Energy Environ. Sci.* **2015**, *8*, 1905−1922.
(31) Biesinger, M. C.; Lau, L. W. M.; Gerson, A. R.; Smart, R. S. C. Resolving surface chemical states in XPS analysis of first row transition metals, oxides and hydroxides: Sc, Ti, V, Cu and Zn. *Appl. Surf. Sci.* **2010**, *257*, 887−898.
(32) Platzman, I.; Brener, R.; Haick, H.; Tannenbaum, R. Oxidation of polycrystalline copper thin films at ambient conditions. *J. Phys. Chem. C* **2008**, *112*, 1101−1108.
(33) Yamamoto, S.; Bluhm, H.; Andersson, K.; Ketteler, G.; Ogasawara, H.; Salmeron, M.; Nilsson, A. In situ X-ray photoelectron spectroscopy studies of water on metals and oxides at ambient conditions. *J. Phys.: Condens. Matter* **2008**, *20*, 184025.
(34) Akhavan, O.; Azimirad, R.; Safa, S.; Hasani, E. CuO/$Cu(OH)_2$ hierarchical nanostructures as bactericidal photocatalysts. *J. Mater. Chem.* **2011**, *21*, 9634−9640.
(35) Deng, Y.; Handoko, A. D.; Du, Y.; Xi, S.; Yeo, B. S. In situ Raman spectroscopy of copper and copper oxide surfaces during electrochemical oxygen evolution reaction: identification of Cu^{III} oxides as catalytically active species. *ACS Catal.* **2016**, *6*, 2473−2481.
(36) Shiraishi, S.; Kanamura, K.; Takehara, Z. Influence of initial surface condition of lithium metal anodes on surface modification with HF. *J. Appl. Electrochem.* **1999**, *29*, 867−879.
(37) Kanamura, K. Electrochemical deposition of very smooth lithium using nonaqueous electrolytes containing HF. *J. Electrochem. Soc.* **1996**, *143*, 2187.
(38) Kanamura, K. X-ray photoelectron spectroscopic analysis and scanning electron microscopic observation of the lithium surface immersed in nonaqueous solvents. *J. Electrochem. Soc.* **1994**, *141*, 2379.
(39) Kanamura, K.; Tamura, H.; Shiraishi, S.; Takehara, Z. XPS analysis of lithium surfaces following immersion in various solvents containing $LiBF_4$. *J. Electrochem. Soc.* **1995**, *142*, 340−347.

DOI: 10.1021/acs.nanolett.8b03070
Nano Lett. 2018, 18, 7066−7074

(40) Ro, C.; Linton, R. W. Characterization of LiF using XPS. *Surf. Sci. Spectra* **1992**, *1*, 277−283.
(41) Jurng, S.; Brown, Z. L.; Kim, J.; Lucht, B. L. Effect of electrolyte on the nanostructure of the solid electrolyte interphase (SEI) and performance of lithium metal anodes. *Energy Environ. Sci.* **2018**, *11*, 2600.
(42) Arreaga-Salas, D. E.; Sra, A. K.; Roodenko, K.; Chabal, Y. J.; Hinkle, C. L. Progression of solid electrolyte interphase formation on hydrogenated amorphous silicon anodes for lithium-ion batteries. *J. Phys. Chem. C* **2012**, *116*, 9072−9077.
(43) Diao, Y.; Xie, K.; Xiong, S.; Hong, X. Insights into Li-S battery cathode capacity fading mechanisms: irreversible oxidation of active mass during cycling. *J. Electrochem. Soc.* **2012**, *159*, A1816−A1821.
(44) Nasybulin, E.; Xu, W.; Engelhard, M. H.; Nie, Z.; Burton, S. D.; Cosimbescu, L.; Gross, M. E.; Zhang, J.-G. Effects of electrolyte salts on the performance of Li-O_2 batteries. *J. Phys. Chem. C* **2013**, *117*, 2635−2645.
(45) Yamamura, Y.; Tawara, H. Energy dependence of ion-induced sputtering yields from monatomic solids at normal incidence. *At. Data Nucl. Data Tables* **1996**, *62*, 149−253.
(46) Chambers, G. P.; Fine, J. *Practical surface analysis: ion and neutral spectroscopy*, 2nd ed.; Briggs, D., Seah, M. P., Eds.; John Wiley: New York, 1992; Vol. *2*, 1−756.
(47) Veisfeld, N.; Geller, J. D. Ion sputtering yield measurements for submicrometer thin films. *J. Vac. Sci. Technol., A* **1988**, *6*, 2077.

DOI: 10.1021/acs.nanolett.8b03070
Nano Lett. 2018, 18, 7066−7074